

Self-Assembled Aggregates of Rod-Coil Block Copolymers and Their Solubilization and Encapsulation of Fullerenes

Samson A. Jenekhe* and X. Linda Chen

Amphiphilic poly(phenylquinoline)-*block*-polystyrene rod-coil diblock copolymers were observed to self-organize into robust, micrometer-scale, spherical, vesicular, cylindrical, and lamellar aggregates from solution. These diverse aggregate morphologies were seen at each composition, but their size scale decreased with a decreasing fraction of the rigid-rod block. Compared to coil-coil block copolymer micelles, the present aggregates are larger by about two orders of magnitude and have aggregation numbers of over 10^8 . The spherical and cylindrical aggregates have large hollow cavities. Only spherical aggregates with aggregation numbers in excess of 10^9 were formed in the presence of fullerenes (C_{60} , C_{70}) in solution, resulting in the solubilization and encapsulation of over 10^{10} fullerene molecules per aggregate.

Block copolymers can produce numerous phase-separated microstructures and nanostructures that are of wide scientific and technological interest (1–12). Conventional applications of such block copolymer assemblies include thermoplastic elastomers, pressure-sensitive adhesives, colloidal dispersants, compatibilizers of polymer blends, foams, and surface modification (2–4, 6–8). Of the factors that determine the microstructure of block copolymers, conformational asymmetry between the blocks is perhaps the least understood (5, 11). Theoretical studies of rod-coil block copolymers, in which the ultimate conformational asymmetry is achieved, have predicted major differences in phase behavior, self-assembly, and microstructures compared to flexible coil-coil block copolymers (11). However, only few experimental studies of synthetic rod-coil block copolymers have been reported (5).

We describe the self-assembly from solution, micelle-like aggregate morphologies, aggregate supramolecular structure, and solubilization properties of a synthetic rod-coil diblock copolymer, poly(phenylquinoline)-*block*-polystyrene (PPQ-*b*-PS) (Fig. 1). The heterocyclic rigid-rod polyquinoline block allows tuning of its amphiphilicity. For example, through protonation or quaternization of the imine nitrogen (13), the rodlike block can be turned into a polyelectrolyte. The π -conjugated nature of the rigid-rod block confers electroactive and photoactive properties (13, 14) on the block copolymers while providing novel ways of probing the self-assembly, molecular packing, morphology, and dynamics of the polymeric amphi-

philes by optical and photoelectronic techniques. The amide linkage at the rod-coil interface in each block copolymer chain provides a means of strong intermolecular interactions, through hydrogen bonding, that might enhance the stability of self-organized structures. The PPQ-PS copolymers, in selective solvents for PPQ, form large aggregates with various morphologies (spheres, vesicles, cylinders, and lamellae), which can be observed by optical microscopy. Surprisingly, spherical fullerenes (C_{60} , C_{70}) can be solubilized to a large degree by solutions of the rod-coil block copolymers, resulting in the encapsulation of huge numbers ($\sim 10^{10}$) of fullerene molecules.

The synthesis, purification, and characterization of PPQ_{50} - PS_{300} and PPQ_{10} - PS_{300} (subscripts are the number of monomers per block) are described elsewhere (15). Dilute solutions (0.5 to 1.0 mg/ml) of each diblock copolymer in mixed solvents—trifluoroacetic acid (TFA) and dichloromethane (DCM), or TFA and toluene—at various volume ratios were used for aggregation studies. Because TFA is a good solvent for PPQ block and protonates its imine nitrogens, whereas the PS block is insoluble in it, micelle-like aggregates (Fig. 1) result from manipulation of the solvent composition. The expected structure of such an aggregate in the TFA solution is an inner PS block surrounded by the protonated PPQ shell. This basic aggregate structure is expected to be retained in the solid state after solvent evaporation, which also deprotonates the PPQ block (Fig. 1). The self-assembly of a rod-coil diblock copolymer in a selective solvent for the rigid-rod block has not been theoretically investigated (11) but is experimentally accessible here because of the differential solubility of PPQ and PS blocks. Self-assembly of discrete aggregates of the

rod-coil diblock copolymers did not occur from solutions in nonselective solvents, such as nitromethane containing $GaCl_3$ (15).

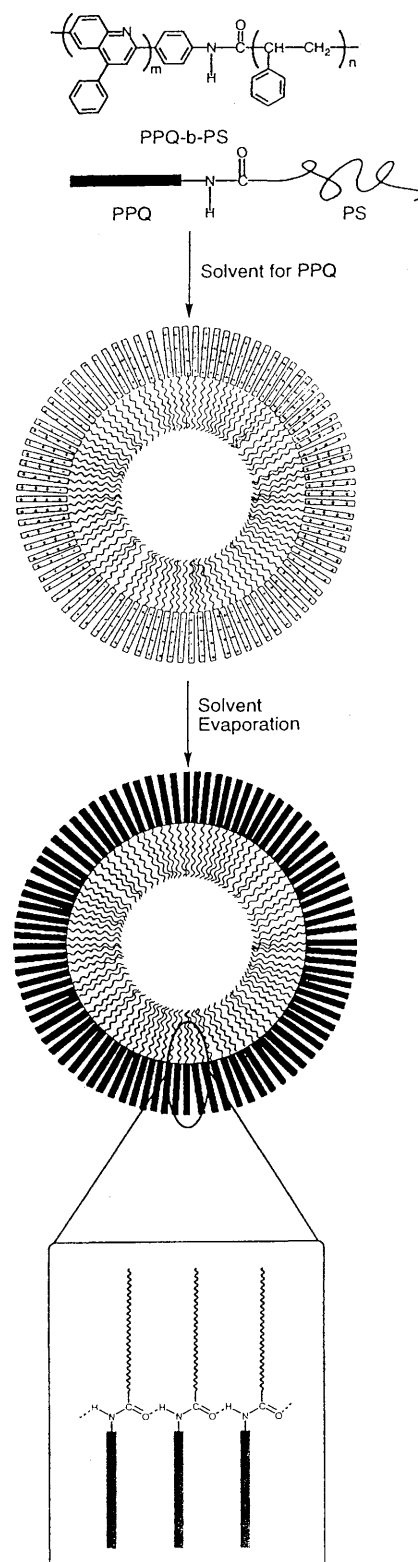


Fig. 1. Chemical structure and schematic illustration of the self-assembly of PPQ-*b*-PS rod-coil diblock copolymers into hollow aggregates.

Departments of Chemical Engineering and Chemistry, University of Rochester, Rochester, NY 14627-0166, USA.

*To whom correspondence should be addressed. E-mail: jenekhe@che.rochester.edu

Four different, micelle-like aggregate morphologies were observed in PPQ₅₀-PS₃₀₀ by optical and scanning electron microscopies: spheres, lamellae, cylinders, and vesicles (Fig. 2). The main factors determining morphology were the initial solvent composition (TFA:DCM ratio) and the solution drying rate. Spherical aggregates with a wide distribution of sizes (typical diameters of 0.5 to 10 μm) were observed after rapid drying of the solutions on a heated substrate at 95°C. Aggregates prepared by drying solutions at room temperature had nonspherical morphologies, and each sample was predominantly (~70%) either lamellae, cylinders, or vesicles, depending on the initial solvent composition; the minor phases in these morphologies were cylinders, lamellae, or spheres, respectively. Lamellar aggregates had diameters between 5 and 30 μm; the cylinders were relatively uniform in diameter (1 to 3 μm) but highly polydisperse in length (5 to 25 μm); and vesicles had outer diameters of about 0.5 to 1.0 μm and wall thickness of about 200 nm. Similar multiple morphologies were observed in aggregates of PPQ₁₀-PS₃₀₀, whose average sizes were all smaller than those of PPQ₅₀-PS₃₀₀ by about a factor of 2. Repeated heating of the aggregates to 200°C, which is above the glass transition temperature (T_g) of PS blocks ($T_g = 100^\circ\text{C}$) and

below that of PPQ blocks ($T_g > 350^\circ\text{C}$) (13), did not have any effect on the aggregate morphologies, which demonstrates the robustness of these aggregates. Also, the polydispersity of the rigid-rod block (15) apparently had no discernible effect on the aggregate morphologies. Compared to recently observed multiple morphologies in coil-coil block copolymers (12), the present aggregates are larger by about two orders of magnitude.

The unusually large sizes of the spherical and cylindrical aggregates—unlike those of bilayer vesicles and lamellae, which could in principle grow to any size—cannot be explained by a simple core-shell structure of conventional block copolymer micelles (3, 6–8, 11, 12). The main difficulty is that the rod-coil block copolymer chains from which the aggregates are assembled have, on average, fully extended lengths of at most ~100 nm (16). Spherical and cylindrical aggregates about 200 nm in diameter are thus expected if solid assemblies of a PS core and PPQ shell were formed. In contrast, the observed aggregates are about 10 to 50 times larger (Fig. 2).

To account for the size difference, we propose that the observed spherical and cylindrical aggregates form large hollow cavities. An aggregate structure in accord with this hypothesis has a cavity core, a PS

inner shell, and a PPQ outer shell (Fig. 1). For a typical 5-μm-diameter spherical aggregate, 89% of its total volume of 65 μm³ is empty. The driving force for the large size and hollow cavity of these aggregates appears to be a more efficient packing of the rigid-rod blocks and, consequently, a more ordered and stable aggregate structure. All of the different aggregates under cross-polarizers showed that they were highly ordered with crystalline features. The aggregation number N_0 , or number of diblock copolymer chains per aggregate, was estimated to be 1×10^8 and 3×10^8 for the spherical and cylindrical aggregates, respectively (17).

The aggregate luminescence of PPQ₅₀-PS₃₀₀ was explored as a means of probing the molecular packing of the luminescent rigid-rod PPQ blocks in the different aggregate morphologies. Different photoluminescence (PL) emission and excitation spectra were observed for spherical, lamellar, and cylindrical aggregates (Fig. 3). A blue emission band with peak at 454 nm for the spherical aggregates can be interpreted as coming from PPQ blocks that are not parallel. In contrast, both lamellar and cylindrical aggregates have broad emission bands with peaks at 576 and 594 nm, respectively, which are close to the PL emission band ($\lambda_{\text{max}} = 578 \text{ nm}$) of the similarly excited PPQ homopolymer thin film (18). The similarity of the emission spectra of the lamellar and cylindrical aggregates to that of the homopolymer, which is known to luminesce through excimer-like aggregates (18, 19), suggests a high degree of close packing of PPQ block chains in the lamellar and cylindrical aggregates. The different molecular packing of PPQ blocks in the spherical and lamellar and cylindrical aggregates is confirmed by the PL excitation spectra monitored at the respective emission peaks (Fig. 3). Whereas the spherical aggregates show an absorption peak at 390 nm, which is similar to the absorption spectrum of the PPQ homopolymer, the lamellar and cylindrical aggregates have two absorption peaks (406 and 423 nm) and a shoulder (~460 nm) in their excitation spectra. Time-resolved PL decay dynamics of the fluorescent PPQ block in the different aggregate morphologies evidenced different excited-state lifetimes (Fig. 3). Compared to the PPQ homopolymer thin film, which exhibits two lifetimes (1.1 and 4.7 ns), the PL decay dynamics of PPQ blocks in the spherical aggregates is approximately described by a single lifetime of 0.93 ns. However, in the lamellar and cylindrical aggregates, biexponential lifetimes of 0.38 and 3.5 ns and 0.34 and 2.6 ns, respectively, best fit the decay dynamics. These results suggest that the observed morphology-dependent emission

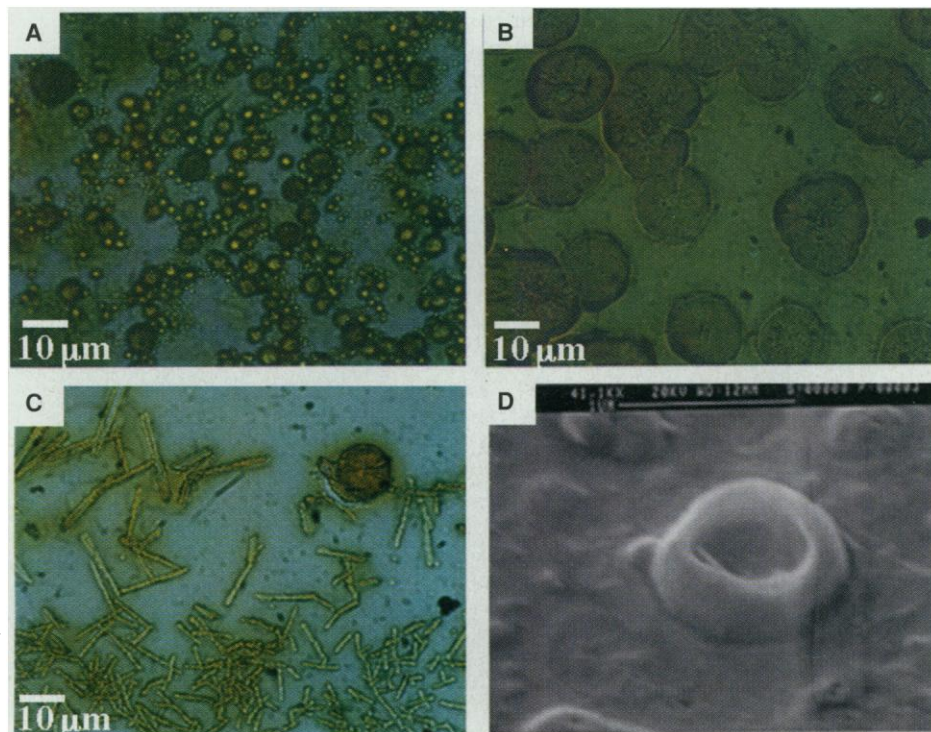


Fig. 2. Optical (A to C) and scanning electron (D) micrographs of the typical morphologies of PPQ₅₀-PS₃₀₀. Drops of dilute solutions (0.5 to 1.0 mg/ml) of the diblock copolymers were spread and dried on glass slides and aluminum substrates, respectively. (A) Spherical aggregates (1:1 TFA:DCM, v/v, 95°C); (B) lamellae (1:1 TFA:DCM, 25°C); (C) cylinders (9:1 TFA:DCM, 25°C); and (D) vesicles (1:1–1:4 TFA:DCM, 25°C).

properties of the block copolymer aggregates reflect the varied molecular packing of the fluorescent rigid-rod block.

Fluorescence photomicrographs (Fig. 4) confirmed the aggregate sizes and shapes observed by optical and scanning electron microscopies and revealed that the fluorescent rigid-rod blocks are located at the outer shells of the aggregates, as depicted in the model of Fig. 1. The hollow microcavity and closed ends of the cylindrical aggregates were also revealed (Fig. 4C). The entire ~200-nm bilayer thickness of each vesicle appears to fluoresce because the ~140-nm separation between the PPQ blocks in the bilayers is below the resolution limit (Fig. 4D). Also, because of three-dimensional (3D) symmetry and uniformity of emission, the microcavity of the spherical aggregates could not be directly observed (Fig. 4A) but can be inferred from that of similarly formed cylinders (Fig. 1). The 3D nature of the spherical aggregates can be clearly distinguished from the relatively flat (2D) lamellae, which have rough surfaces.

The large sizes, aggregation numbers, and microcavities of these micelle-like aggregates suggest that the block copolymer assemblies in solution might be capable of solubilizing large molecules or encapsulating nanoparticles. We studied the solubilization of the fullerenes C_{60} and C_{70} because of their large sizes and generally poor solubility (20–22) and the prospect of preparing block copolymer aggregates with encapsulated fullerenes. Although some guest-host complexes of C_{60} with γ -cyclodextrin (23), calixarenes (24), and hydroquinone (25) have been reported, few host molecules have cavities large enough to encase one molecule of C_{60} or the higher fullerenes (20, 26). Although C_{60} is slightly soluble in pure DCM (0.254 mg/ml, 0.192 mg/g) and pure toluene (2.8 mg/ml, 3.16 mg/g) at 22° to 30°C (20–22), both C_{60} and C_{70} were insoluble in pure TFA, TFA-DCM, and TFA-toluene (1:1 mixtures, v/v). However, both fullerenes were soluble in the mixed solvents containing PPQ₅₀-PS₃₀₀ or PPQ₁₀-PS₃₀₀ diblock copolymer at 25°C, demonstrating the solubilization of C_{60} and C_{70} in the block copolymer aggregates.

These spherical aggregates with solubilized fullerenes (5 weight %) from TFA-DCM (Fig. 5A) and TFA-toluene (Fig. 5B) have typical diameters in the 15 to 30 μm range, about a factor of 3 larger than those of the average pure block copolymer aggregates. The size of the spherical aggregates increased as the amount of fullerene incorporated increased from 1 weight % to the solubility limit of 6 weight %. The corresponding solubilization capacities at 5 and 6 weight % are 3 and 3.7 fullerene molecules per diblock chain, respectively. At 7 to 10

weight % fullerene (C_{60} or C_{70}) or higher, optical microscopy showed the coexistence of the discrete spherical aggregates with additional needle-like and continuous fullerene phases.

Our proposed structure of the spherical rod-coil block copolymer aggregates with

encapsulated fullerenes (Fig. 5C) assumes that the microcavity as well as the inner shell of PS blocks are partially filled with fullerene molecules, whereas the rigid-rod PPQ outer shell blocks are free of fullerenes. Exclusion of fullerene from the rigid-rod shell is reasonable because of the available

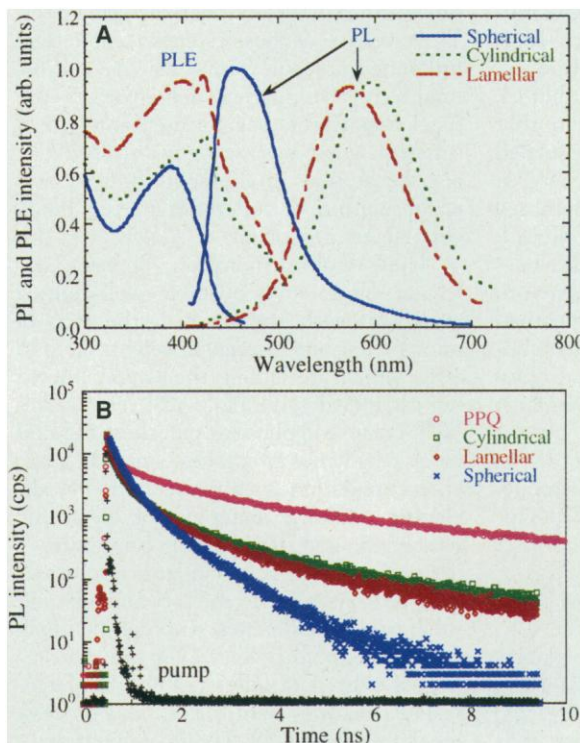


Fig. 3. (A) Photoluminescence (PL) emission and excitation (PLE) spectra and (B) PL decay dynamics of spherical, lamellar, and cylindrical aggregates of PPQ₅₀-PS₃₀₀. The PL emission spectra are for 380-nm excitation, and the PLE spectra were obtained by monitoring the emission peaks (all intensities are in arbitrary units). The PL decay data are for 380-nm laser excitation in time-correlated single-photon counting experiments (cps, counts per second) (15).

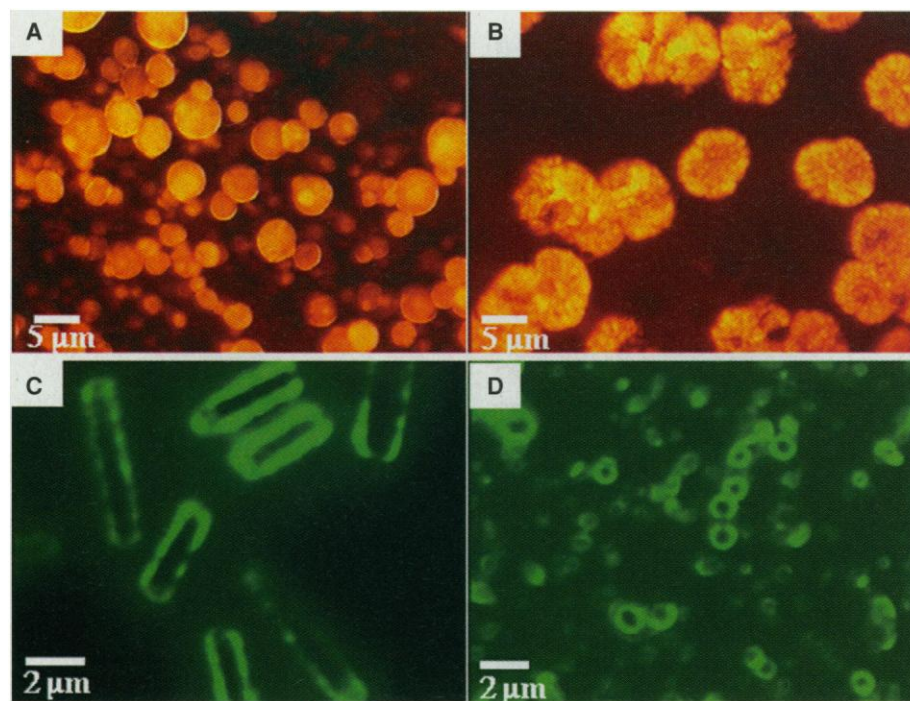


Fig. 4. Fluorescence photomicrographs of the PPQ₅₀-PS₃₀₀ aggregates shown in Fig. 2. (A) Spherical, (B) lamellar, (C) cylindrical, and (D) vesicular aggregates.

microcavity, compatibility with PS, and the difficulty of packing spherical molecules with the rodlike blocks. Optical microscopy of aggregates containing fullerenes under cross-polarizers evidenced a highly ordered and crystalline structure (Fig. 5B). We estimate N_0 for aggregates containing 5 and 6 weight % C_{60} to be of order 6×10^9 and 2×10^{10} , respectively (17). Upon solubilization of the fullerenes, N_0 increased significantly. These aggregation numbers, combined with the observed solubilization capacities of fullerene molecules per diblock chain at 5 and 6 weight %, mean that $>10^{10}$ fullerene molecules are encapsulated in each block copolymer aggregate of Fig. 5.

The observed 64 mg of solubilized fullerene (C_{60} or C_{70}) per gram of diblock copolymer represents a solubility enhancement by factors of 330 and 20 compared to those in pure DCM and toluene, respectively. The best previously reported C_{60} solubility in a solvent is 42.7 mg/g, for 1-chloronaphthalene (21, 22). The observed large solubilization capacity of the block copolymer assemblies for the fullerenes can be partly understood in terms of thermodynamic theory of solubilization (9). The similarity of the solubility parameters of fullerene- C_{60} (δ_f) and polystyrene (δ_{ps}) at 25°C is expected to give a small value of the Flory-Huggins interaction parameter $\chi_{f,ps}$, expressed in terms of the solubility parameters (9). From the reported $\delta_f = 10$ for C_{60} at 25°C (20) and $\delta_{ps} = 8.7$ to 9.9 (9), $\chi_{f,ps} = (\delta_f - \delta_{ps})^2 v_f / k_B T \sim 0.015$, where v_f is molar volume, k_B is the Boltzmann con-

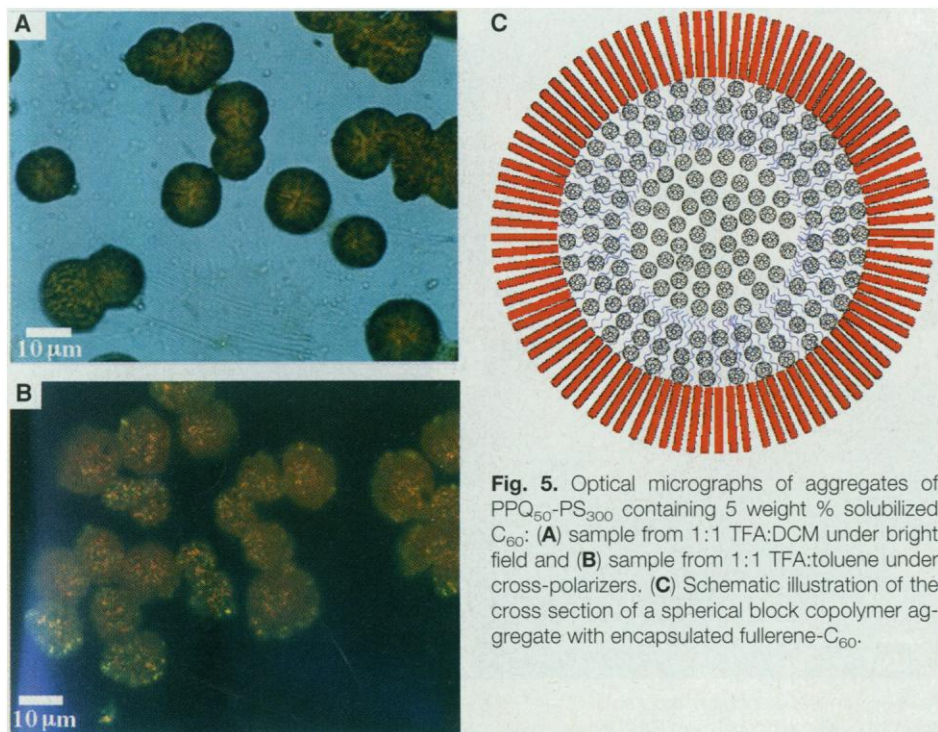
stant, and temperature $T = 298$ K. Correlation of C_{60} solubility to the solubility parameter of many solvents has shown that the largest solubility was observed in solvents with solubility parameters close to that of C_{60} (20, 21). However, one of the most remarkable effects of the introduction of C_{60} or C_{70} into the amphiphilic block copolymer solution is the preferential self-assembly of spherical aggregates. The presence of these essentially spherical fullerene molecules inhibits the self-assembly of nonspherical aggregates of the block copolymers, suggesting that a type of spherical guest-host recognition (26) may also be at play in the solubilization and encapsulation of fullerenes in the block copolymers aggregates.

These results demonstrate the macromolecular self-assembly of stable, well-defined aggregates with size scale in the tens of micrometers and molecular weights of up to 10^{13} , which are among the largest known self-assembled nonbiological structures (27). Possible applications for these rod-coil block copolymer assemblies—including microencapsulation, catalyst support, low dielectric constant materials for electronic packaging, and lightweight composites—derive from their sizes and large microcavities (28). As tunable microcontainers and solubilizers of fullerenes, amphiphilic block copolymers hold potential for the preparation of clusters of fullerenes and the large-scale extraction, purification, and processing of fullerenes (20). Their combination of electroactive and photoactive properties

with self-assembly, robustness, and discrete micrometer-scale particles suggests electrophotographic imaging (29) and other optoelectronic applications (14).

REFERENCES AND NOTES

- M. Muthukumar, C. K. Ober, E. L. Thomas, *Science* **277**, 1225 (1997); Z.-R. Chen, J. A. Kornfield, S. D. Smith, J. T. Grothaus, M. M. Sattkowski, *ibid.*, p. 1248; M. Park, C. Harrison, P. M. Chaikin, R. A. Register, D. H. Adamson, *ibid.* **276**, 1401 (1997).
- F. S. Bates, *ibid.* **251**, 898 (1991); S. T. Milner, *ibid.*, p. 905; G. H. Fredrickson and F. S. Bates, *Annu. Rev. Mater. Sci.* **26**, 501 (1996).
- A. Halperin, M. Tirrell, T. P. Lodge, *Adv. Polym. Sci.* **100**, 31 (1992); M. Tirrell, *ibid.*, pp. 281–308.
- A. Noshay and J. E. McGrath, *Block Copolymers: Overview and Critical Survey* (Academic Press, New York, 1977).
- J. T. Chen, E. L. Thomas, C. K. Ober, G.-P. Mao, *Science* **273**, 343 (1996); J. T. Chen, E. L. Thomas, C. K. Ober, S. S. Hwang, *Macromolecules* **28**, 1688 (1995); L. H. Radzilowski, J. L. Wu, S. I. Stupp, *ibid.* **26**, 879 (1993); L. H. Radzilowski and S. I. Stupp, *ibid.* **27**, 7747 (1994); G. Widawski, M. Rawiso, B. François, *Nature* **369**, 387 (1994); D. Vemino, D. Tirrell, M. Tirrell, *Polym. Mater. Sci. Eng.* **71**, 496 (1994).
- Z. Tuzar and P. Kratochvil, *Surf. Colloid Sci.* **15**, 1 (1993).
- S. E. Weber, P. Munk, Z. Tuzar, Eds., *Solvents and Self-Organization of Polymers* (Kluwer Academic, Dordrecht, Netherlands, 1996).
- A. P. Gast, in (7), pp. 259–280; L. J. M. Vagberg, K. A. Cogan, A. P. Gast, *Macromolecules* **24**, 1670 (1991).
- R. Nagarajan, M. Barry, E. Ruckenstein, *Langmuir* **2**, 210 (1986); R. Nagarajan, in (7), pp. 121–165.
- X. L. Chen and S. A. Jenekhe, *Macromolecules* **29**, 6189 (1996); *Appl. Phys. Lett.* **70**, 487 (1997).
- A. N. Semenov and S. V. Vasilenko, *Sov. Phys. JETP* **63**, 70 (1986); A. N. Semenov, *Mol. Cryst. Liq. Cryst.* **209**, 191 (1991); A. Halperin, *Macromolecules* **23**, 2724 (1990); *Europhys. Lett.* **10**, 549 (1989); D. R. M. Williams and G. H. Fredrickson, *Macromolecules* **25**, 3561 (1992); E. Raphael and P. G. de Gennes, *Makromol. Chem. Macromol. Symp.* **62**, 1 (1992).
- L. Zhang, K. Yu, A. Eisenberg, *Science* **272**, 1777 (1996); L. Zhang and A. Eisenberg, *ibid.* **268**, 1728 (1995); *J. Am. Chem. Soc.* **118**, 3168 (1996).
- P. D. Sybert, W. H. Beever, J. K. Stille, *Macromolecules* **14**, 493 (1981); A. K. Agrawal and S. A. Jenekhe, *ibid.* **26**, 895 (1993); *Chem. Mater.* **8**, 579 (1996).
- S. A. Jenekhe and K. J. Wynne, Eds., *Photonic and Optoelectronic Polymers* (American Chemical Society, Washington, DC, 1997).
- For details on the synthesis, characterization, and aggregation experiments on PPQ-b-PS block copolymers, see the supplementary material available at www.sciencemag.org/feature/data/976170.shl. For details on our photoluminescence experimental techniques, see J. A. Osaheni and S. A. Jenekhe, *J. Am. Chem. Soc.* **117**, 7389 (1995).
- From x-ray diffraction data on oligoquinolines (A. S. Shetty *et al.*, in preparation), the repeat unit length of PPQ is 0.64 nm. We estimate the repeat unit length of extended-chain PS to be ~ 0.226 nm. Therefore, the maximum extended-chain lengths of PPQ₅₀-PS₃₀₀ and PPQ₁₀-PS₃₀₀ will be ~ 100 and ~ 74 nm, respectively.
- The order of magnitude of N_0 was estimated as follows. About 2×10^5 discrete spherical aggregates per square millimeter were measured from a photomicrograph taken from a 1-mg diblock copolymer sample covering a total area of 5 cm². Thus, one gets 2.4×10^{-16} mol (or 10^{-8} mg) of diblock per aggregate or $N_0 = 1.5 \times 10^8$. For a typical 5- μ m-diameter spherical aggregate with a volume of 65 μ m³ that is 89% empty, assuming an aggregate density of 0.2 g/cm³ gives $N_0 = 2 \times 10^8$, in agreement with the direct experimental estimate. Similar



- procedures for cylindrical aggregates gave 2×10^4 aggregates/mm² from a photomicrograph taken on a 0.2-mg diblock copolymer sample covering 5 cm². From this calculation, one gets 4.8×10^{-15} mol of diblock per aggregate or $N_0 = 3 \times 10^9$. In the case of PPQ₅₀-PS₃₀₀ aggregates containing 5 weight % solubilized C₆₀, 10³ spherical aggregates/mm² were measured from a photomicrograph taken from a 0.2-mg diblock-C₆₀ sample covering 5 cm². From this information, one gets 9.6×10^{-15} mol of diblock per aggregate or $N_0 = 6 \times 10^9$. Similarly, for the case of aggregates containing 6 weight % C₆₀, $N_0 = 2 \times 10^{10}$.
18. S. A. Jenekhe *et al.*, *Chem. Mater.* **9**, 409 (1997).
 19. S. A. Jenekhe and J. A. Osaheni, *Science* **265**, 765 (1994).
 20. M. S. Dresselhaus, G. Dresselhaus, P. C. Eklund, *Science of Fullerenes and Carbon Nanotubes* (Academic Press, San Diego, CA, 1996).
 21. R. S. Ruoff, D. S. Tse, R. Malhotra, D. C. Lorents, *J. Phys. Chem.* **97**, 3379 (1993).
 22. N. Sivaraman *et al.*, *J. Org. Chem.* **57**, 6077 (1992).
 23. T. Andersson, K. Nilsson, M. Sundahl, G. Westman, O. Wennerstrom, *J. Chem. Soc. Chem. Commun.* **1992**, 604 (1992).
 24. J. L. Atwood, G. A. Koutsantonis, C. L. Raston, *Nature* **368**, 229 (1994).
 25. O. Ermer and C. Robke, *J. Am. Chem. Soc.* **115**, 10077 (1993).
 26. J.-M. Lehn, *Supramolecular Chemistry* (VCH, New York, 1995).
 27. G. M. Whitesides, J. P. Mathias, C. T. Seto, *Science* **254**, 1312 (1991).
 28. D. L. Wilcox Sr., M. Berg, T. Bernat, D. Kellerman, J. K. Cochran Jr., Eds., *Hollow and Solid Spheres and Microspheres: Science and Technology Associated with Their Fabrication and Application* (MRS Proc. 372, Materials Research Society, Pittsburgh, PA, 1995); S. Benita, Ed., *Microencapsulation: Methods and Industrial Applications* (Dekker, New York, 1996).
 29. D. M. Pai and B. E. Springett, *Rev. Mod. Phys.* **65**, 163 (1993); J. A. Osaheni, S. A. Jenekhe, J. Perlstein, *J. Phys. Chem.* **98**, 12727 (1994).
 30. We thank A. S. Shetty for helpful discussion and technical assistance. This research was supported by the Office of Naval Research and in part by the National Science Foundation (grants CTS-9311741 and CHE-9120001).

13 November 1997; accepted 2 February 1998

Inducing and Viewing the Rotational Motion of a Single Molecule

B. C. Stipe, M. A. Rezaei, W. Ho*

Tunneling electrons from the tip of a scanning tunneling microscope were used to induce and monitor the reversible rotation of single molecules of molecular oxygen among three equivalent orientations on the platinum(111) surface. Detailed studies of the rotation rates indicate a crossover from a single-electron process to a multielectron process below a threshold tunneling voltage. Values for the energy barrier to rotation and the vibrational relaxation rate of the molecule were obtained by comparing the experimental data with a theoretical model. The ability to induce the controlled motion of single molecules enhances our understanding of basic chemical processes on surfaces and may lead to useful single-molecule devices.

It is conceivable that, at the limit of miniaturization, individual atoms and molecules will physically constitute useful devices and their quantum properties will specify the desired functions and performance. A demonstration of such an atomic-scale electronic device was a reversible atomic switch that used a scanning tunneling microscope (STM) (1). In this experiment, a single Xe atom was transferred reversibly between the W tip of the STM and a Ni surface by the application of a voltage between them, resulting in bistable values of the tunneling current. A single-atom switch has also been demonstrated for Si adatoms on the Si(111)-7×7 surface where an atom was moved between two specific sites on the surface (2). The STM has been used to perform atomic-scale manipulation by a variety of other methods (3, 4), including the pushing or pulling of single atoms and molecules on a surface with the STM tip (5–8). By scanning regions of the Si(100)-(2×1) surface at high sample bias, it was possible to observe the reversible rotation of adsorbed Sb dimers between two stable orientations (9).

Using the basic method described in the atomic switch experiments (1, 2), we have studied the reversible rotation of single O₂ molecules among three equivalent orientations on the Pt(111) surface by accurately positioning the tip above the molecule and monitoring the rapid changes in tunneling current as the molecule rotates. Monitoring the tunneling current allows us to freeze the motion of the molecule in any chosen orientation and to compile statistics for the distribution of times spent in each orientation. The time dependence of the tunneling current yields a quantitative measure of the rotation rate and of the way in which this rate varies with the applied voltage and current. These studies show that the rotation is caused by the inelastic tunneling of low-energy electrons. The results provide insight into the adsorption and excitation properties of the molecule, including a value for the energy barrier to rotation.

The system O₂ on Pt(111) has been studied extensively because of the importance of Pt as a catalyst in oxidation reactions. Two chemisorbed O₂ species have been identified on Pt(111) below 100 K with the use of electron energy loss spectroscopy (EELS) (10, 11). The O–O bond for both species was determined by near-edge x-ray absorption fine structure spectroscopy to be aligned parallel or nearly

parallel to the surface (12). With the STM, we have recently identified the adsorption sites of these species and have discovered a third type at step edges (13). The subject of the present work is the species responsible for the 87-meV O–O stretch vibration observed in EELS (11). The STM images in Fig. 1 show these molecules as having a “pear” shape centered on the face-centered cubic (fcc), threefold hollow sites of the surface, with the bright lobe over a top site and the smaller, dimmer lobe over the opposite bridge site. By symmetry, they have three equivalent orientations separated by 120°.

Details of the homemade STM and experimental setup have been described elsewhere (14). We find the adsorption dynamics of O₂ on Pt(111) to be complex (13) because of the existence of a mobile precursor to chemisorption, whose lifetime and route to chemisorption are sensitive functions of temperature (14). In order to favor the adsorption of isolated O₂, the clean Pt(111) surface was exposed to O₂ at 85 K until a coverage of approximately 0.01 monolayer was observed. The surface was then cooled to 8 K to minimize temperature-induced effects. We rotated molecules by applying a voltage pulse to the sample while the tunneling current was recorded. Data shown in this report are for positive voltage pulses applied to the sample. An iterative tracking scheme was used to position the W tip at a chosen point above a molecule with lateral and vertical resolutions of 0.1 and 0.01 Å, respectively. We did this by searching out a local maximum or minimum of the tip height with the STM's feedback loop turned on to maintain constant tunneling current. Lateral offsets were added to give the desired tip position during the pulse. Feedback was then turned off, and the tip was moved vertically to give the desired initial current. The tip remained stationary during the voltage pulse.

After imaging an isolated O₂ molecule (Fig. 1A), we positioned the STM tip directly over the brightest point of the molecule where the tunneling current is at its

Laboratory of Atomic and Solid State Physics and Materials Science Center, Cornell University, Ithaca, NY 14853, USA.

*To whom correspondence should be addressed. E-mail: wilsonho@msc.cornell.edu